# A high-performance Ti-Zr Based Chromium-Free Conversion Coating on 2024 Aluminum Alloy

*Q.P. Li* [1,2,*], *Z.Q. Yan* [2,3], *Q. Xu* [1], *B. Zhang* [2], *S. Sun* [3], *J.G. Liu* [2], *C.W. Yan* [2]

[1] School of Metallurgy, Northeastern University, Shenyang 110142
[2] Laboratory for Corrosion and Protection, Institute of Metal Research, Chinese Academy of Sciences, Shenyang 110016
[3] School of Science, Shenyang University of Technology Shenyang 110870
*E-mail: qpli@imr.ac.cn

In order to further improve the corrosion resistance of the chromium-free Ti-Zr conversion coating on 2024 aluminum alloy (AA2024), a novel Ti-Zr based conversion coating on AA2024 is successfully prepared by introducing the cathodic inhibitor of benzimidazole into the Ti-Zr conversion solution. After the conversion treatment, AA2024 substrate is well covered with the porous Ti-Zr conversion coating composed of the micron-sized particles. And the Ti-Zr conversion coating mainly consists of the metallic oxide ($TiO_2$, $ZrO_2$, $Al_2O_3$), metallic fluoride ($ZrF_4$ and $AlF_3$) and C-N complex. More important is that there are no apparent corrosion products or detects could be observed during the whole 168 h NSS test, indicating the significantly excellent corrosion resistance for AA2024 with Ti-Zr conversion coating compared with other chrome-free conversion coatings. The electrochemical measurements indicate the corrosion resistance of the Ti-Zr conversion coating is not so outstanding at the initial stage, what is worth cherishing is that its anti-corrosion property is gradually improving in the following period. Therefore, the Ti-Zr conversion coating with excellent corrosion resistance might be a promising high-performance protective coating for AA2024 compared with other chrome-free conversion coating.

## 1. INTRODUCTION

Due to its high strength and fatigue resistance, 2024 aluminum alloy (AA2024) is widely used in aircraft structures, especially wing and fuselage structures under tension [1-3]. The copper and other alloying elements such as magnesium, zinc, manganese, silicon or iron contained in AA2024 play an important role in improving its strength, while their existence also makes the AA2024 susceptible to

localized corrosion [2]. To resolve the issue of the localized corrosion, a suitable protection coating must be applied to the alloy surfaces. Chromate conversion coatings have been extensively used as anticorrosive treatments in the aircraft industry for over 50 years because of their self-healing ability, active corrosion protection and excellent adhesive forces to the alloy surface [4,5]. However, hexavalent chromium in the chromate conversion coating is highly toxic and carcinogenic, which results in the serious environmental pollution directly [1,2]. Therefore, the development of an environment-friendly chrome-free chemical conversion coating will become the inevitable trend of the protection techniques of AA2024.

Up to now, some environment-friendly chrome-free chemical conversion techniques, such as molybdates, silicate, rare earth salt, permanganate, phosphate and titanate conversion coating [6-9], have been developed by the pioneers. But none of the above-mentioned chromium-free chemical conversion technologies exhibit a comparable corrosion resistance with the chromate treatment technology. It is worth noting that Titanium or (and) Zirconium chrome-free chemical conversion coating on different aluminum alloy have been developed by many researchers in last few years [9-11], and its preferable corrosion resistance compared with other non-chromium chemical conversion coatings makes it considered to be the most promising candidate instead of the chromate conversion coatings. Even so, the corrosion resistance of the Ti-Zr chrome-free conversion coatings on AA2024 is still not satisfactory especially in the high copper content of 2 and 7 series aluminum alloy surface and it is necessary to pay more attentions to their further optimized improvement in the formulation and technology [1-3].

Recently, plenty of inorganic additives such as $H_3BO_3$, NaF, HF and $NaBF_4$ were used as the coating-formation accelerant which could raise the forming speed of the chrome-free conversion coatings greatly [12]. In addition, some organic additives such as poly(acrylic acid) (PAA), poly(acrylamide) (PAM) and tannic acid (TA) as the inhibitors were also added into the chrome-free conversion coatings with the purpose of improving their corrosion resistance or solving their fatal characteristic of the colorlessness [13]. Indeed, the anti-corrosion performance of the Ti-Zr conversion coatings is improved to some extent after the above-mentioned modifications, however, there is still a gap between the overall corrosion resistance of the Ti-Zr chrome-free treatment and chromate technology, which greatly limits their commercial application.

Just as mentioned above, the pitting and/or intercrystalline corrosion, which might destroy the completeness of the Ti-Zr conversion coatings and further reduce the corresponding corrosion resistance [3], is incident for AA2024 because of the relatively high content of copper, so the Ti-Zr conversion coatings will exhibit more favorable corrosion resistance if the copper in AA2024 is covered or isolated. As typical adsorption-type corrosion inhibitors, the azole-based materials such as benzimidazole and benzotriazole are widely used as the copper corrosion inhibitors in acidic and/or neutral mediums [14], and Recloux also demonstrated the silica mesoporous thin films full of benzotriazole revealed a slowing down of corrosion processes for AA2024 [15]. Accordingly, a novel Ti-Zr based chromium-free conversion coating was developed by adding benzimidazole into the conversion solution to further improve its corrosion resistance on AA2024. And the surface morphology, compositions of the Ti-Zr conversion coating in addition to its corrosion resistance were

investigated systemically with the physico-chemical characterizations and electrochemical measurements.

## 2. EXPERIMENTAL

### 2.1. Preparation of the Ti-Zi conversion coating

AA2024 with the chemical composition (wt. %) of Al (> 92.5), Cu (4.65), Mg (1.63), Mn (0.56), Fe (0.28), Si (0.13), Zn (<0.2) was used as the substrate in this study. Herein, the samples of AA2024 panel with the size of 100 mm (L) × 50 mm (W) × 1 mm (H) were used for the neutral salt spray (NSS) test, immersion test and following electrochemical measurements. Specifically, little samples with the size of 10 mm (L) × 10 mm (W) × 1 mm (H) cut from the above-mentioned big panels were employed for the physicochemical characterizations.

Before the conversion treatment, the specimens were polishing step by step with waterproof abrasive papers with 400 #, 800 # and 1000 # respectively. And then they were degreased with the blended solutions of NaOH (25 g L$^{-1}$), Na$_2$CO$_3$ (20 g L$^{-1}$) , Na$_3$SiO$_4$ (5 g L$^{-1}$) and surfactant (1 g L$^{-1}$) for 4 mins, and then activated in the HF(10 g L$^{-1}$), HNO$_3$ (10 g L$^{-1}$), HCl (10 g L$^{-1}$) and H$_2$SO$_4$ (60 g L$^{-1}$) mixed solutions for 3 mins, and after these steps all the specimens were rinsed with distilled water.

In addition, the main components and corresponding content of conversion solution were as follows: H$_2$TiF$_6$ 3.0～5.0 g L$^{-1}$, H$_2$ZrF$_6$ 1.0~2.0 g L$^{-1}$, benzimidazole 0.1~0.5 g L$^{-1}$, accelerant 0.5~1.0 g L$^{-1}$, oxidizing agent 2.0~3.0 g L$^{-1}$, pH of the conversion solution is between 4~5. After the preparation of the conversion solution, half of the specimens were immersed in the conversion solution at room temperature for 10 mins, and then removed the specimens from conversion solution to air. After drying in air for 1 h, samples with Ti-Zr conversion coating were washed with distilled water to removing the residual bath and placed in the drying oven for standby.

### 2.2. Physicochemical and electrochemical characterizations

The visual surface morphology of the as-prepared samples was observed using a normal optical camera (Sony H10, Japan) and the corresponding micro-structure morphology was obtained with the scanning electron microscope (SEM, FEI XL30, Japan). In addition, the main compositions of the conversion coatings were also analyzed with the energy dispersive spectroscopy (EDS) which is coupled with SEM. X-ray photoelectron spectroscopy (XPS, ESCALAB 250) was also conducted to analyze the surface elements using Mg-Ka radiation (1253 eV, 250 W) under a pressure of ca. 10$^{-7}$ Pa. All binding energy values were calibrated to the C1s graphitic peak at 284.7 eV.

Moreover, the salt spray tests of AA2024 with Ti-Zr conversion coating were conducted in HDYW-120 salt spray chamber for 168 h according to the ASTM B117. Bare (non-coated) substrates were also tested as comparison. The samples during the salt spray tests were taken out to observe the corrosion morphology at a certain intervals. Furthermore, the immersion tests of AA2024 with and without Ti-Zr conversion coating were carried out in 5 wt. % NaCl aqueous solution to estimate the

corresponding corrosion resistance. A conventional three electrodes cell was used for all the electrochemical tests. To be specific, the as-prepared samples with an effective area of 1.7 cm$^2$ use as the working electrodes, a 4 cm$^2$ platinum plate serves as the counter electrode and a saturated calomel electrode (SCE) along with a salt bridge full of saturated potassium chloride solution acts as the reference electrode. All electrochemical measurements were carried out with an EG&G M273 potentiostat and a 5208 two-phase lock-in amplifier at ambient temperature. In addition, 5 wt. % NaCl aqueous solution was prepared to serve as the electrolyte and all the samples were kept immersing in this solution before the electrochemical measurements.

Potentiodynamic polarization measurements were performed with the polarization range of -0.25–0.6 V versus the open circuit potential and the scanning rate was 0.5 mV s$^{-1}$. The electrochemical impedance spectroscopy (EIS) was measured for the samples at the open circuit potential with ±10 mV potential amplitude and a frequency range of 100 kHz-10 mHz. All the EIS data were analyzed by the Solartron Z-View software version 2.2.

## 3. RESULTS AND DISCUSSION

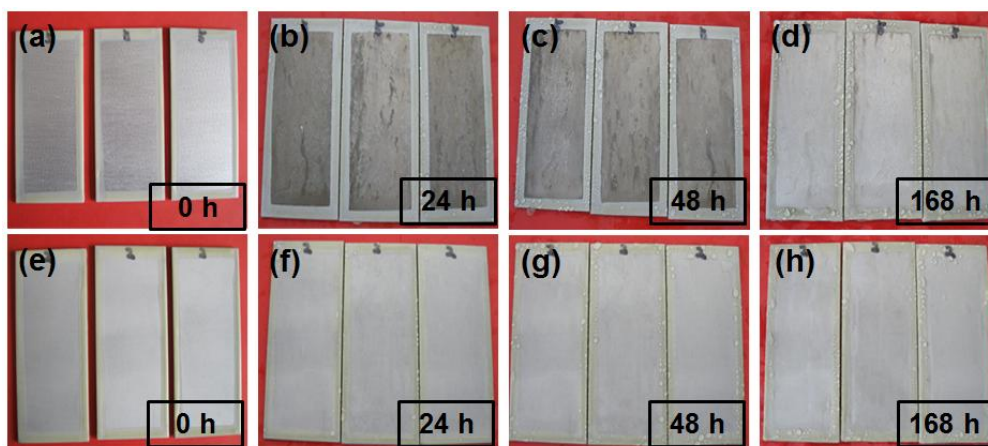*3.1 Physico-chemical characterizations*



**Figure 1.** Photographs of AA2024 substrate (a-d) and AA2024 with Ti-Zr conversion coating (e-h) suffering the NSS test with different times.

Firstly, visual observation of AA2024 substrate and AA2024 with Ti-Zr conversion coating suffering the NSS test with different times was conducted to evaluate the corresponding corrosion resistance qualitatively. As shown in Fig. 1, both AA2024 substrate (Fig. (a)) and AA2024 with Ti-Zr conversion coating (Fig. (e)) before the NSS test seem relatively smooth and there are not any defects or black spots at the surface. However, an obvious corrosion could be seen at the surface of AA2024 substrate with the NSS test of 24 h and lots of black spots generated on the surface of the specimen (Fig. 1(b)). It is worth noting that a relatively smooth surface could be obtained for AA2024 with Ti-Zr conversion coating even if the NSS time increased from 24 to 168 h (Fig. (f-h)), and no apparent

corrosion products or detects could be observed during the whole NSS test except for the negligible dark fringe for the specimen with a 168 h NSS test (Fig. (h)), indicating the significantly excellent corrosion resistance for AA2024 with Ti-Zr conversion coating compared with other chrome-free conversion coating reported in the previous literatures [3,16]. It is curious that the corrosion products decrease gradually for AA2024 substrate with the NSS time increased from 24 to 168 h (Fig. (b-d))), and even a relatively smooth surface with some dark fringes could be obtained again when the NSS time increased to 168 h (Fig. (d)). The exfliation of the corrosion products and re-formation of the relatively complete passivation membrane at the surface of AA2024 substrate during the NSS process might result in the abnormal phenomenon.
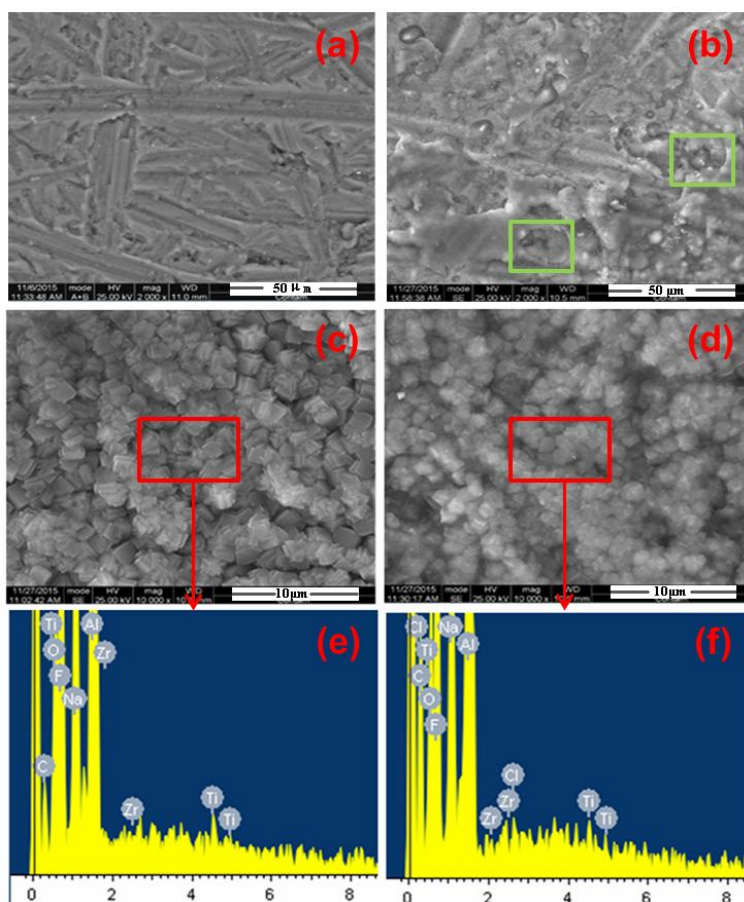


**Figure 2.** SEM images of AA2024 substrate before (a) and after (b) the 168h NSS test; SEM images of AA2024 with Ti-Zr conversion coating before (c) and after (d) the 168 h NSS test and the corresponding EDS spectra (e) and (f).

The surface morphologies of the as-prepared samples before and after the 168 h NSS test are shown in Fig. 2. As shown in Fig. 2(a), lots of scratches could be seen at the surface of AA2024 substrate, which means that the superficial passivation coating was destroyed and the metal aluminum was exposed to the air after the polishment. However, there are some corrosion products former at the surface of AA2024 substrate after the 168 h NSS test (Fig. 2(b)) and some pittings covered with the

corrosion products (inside the green square in Fig. 2(b)) also could be observed apparently. In contrast to these, the porous Ti-Zr conversion coating composed of the micron-sized particles well cover the AA2024 substrate for the samples before and after the 168 h NSS test (Fig. 2(c) and (d)). Even though there is not any apparent corrosion which could be seen in Fig. 1(h), a small amount of corrosion products were generated after the 168 h NSS test and they are well distributed at the surface of the conversion coating, indicating the corrosion resistance of the Ti-Zr conversion coating starts to degrade after the 168 h NSS test despite its excellent anticorrosive property. In addition, the main elements of the Ti-Zr conversion coating are C，O，F, Ti and Zr according to its EDS spectrum (Fig. 2(e)), and they basically keep unchanged before and after the 168 h NSS test (Fig. 2(e)), suggesting the 168 h NSS test has less negative effect on the conversion coating. As for the Na and Cl in AA2024 with Ti-Zr conversion coating after the 168 h NSS test, they might be attributed to the residual NaCl during the NSS test, while the existence of Na for the Ti-Zr conversion coating should be ascribed to the residual Na during the treatment process. Moreover, the appearances of element Al for AA2024 with Ti-Zr conversion coating before and after the 168 h NSS test might be due to the generated Al complex during the conversion process.
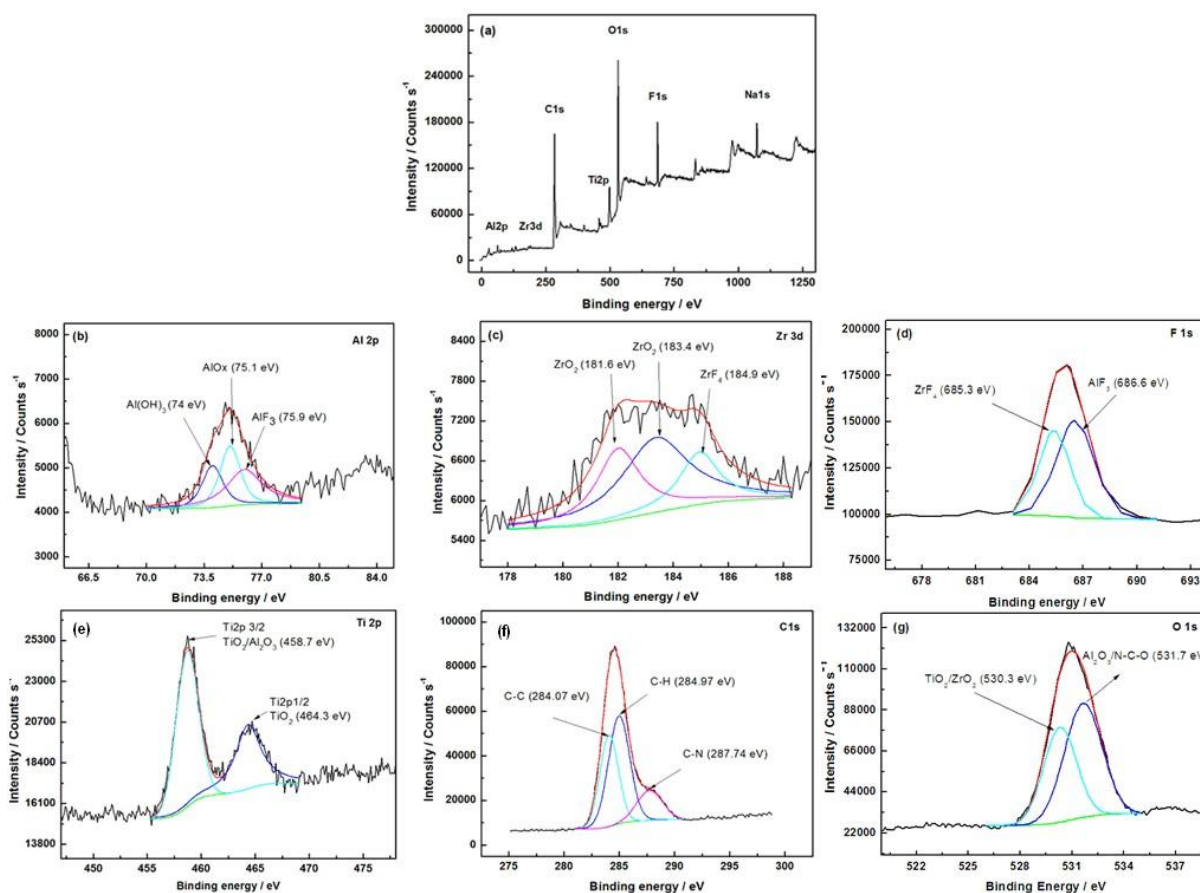


**Figure 3.** XPS spectrum of AA2024 with Ti-Zr conversion coating (a) and the corresponding high resolution de-convoluted spectra of Al 2p (b), Zr 3d (c), F 1s (d), Ti 2p (e), C 1s (f) and O 1s (g).

In order to further investigate the relationship between the compositions, chemical state of the elements in the Ti-Zr conversion coating and its excellent corrosion resistance, XPS spectrum of AA2024 with Ti-Zr conversion coating and the corresponding high resolution de-convoluted spectra of the main elements were analyzed. As shown in Fig. 3(a), it is clear that the major elements of the Ti-Zr conversion coating were C, Ti, O and F along with little amount of Zr and Al. Except for Al and Na which originate from the Al complex and the residual Na as mentioned above, all the elements in the conversion coating come from the conversion solution. Specifically, the peak of C in the XPS spectrum might due to the existence of the introduced benzimidazole.

Furthermore, the main elements of Al, Zr, F, Ti, C and O in the conversion coatings were selected to get high resolution data to further reveal the detailed chemical oxidation state of the elements present in the conversion coating, as shown in Fig. 3(b-g), respectively. The detail of Al 2p (in Fig. 3(b)) reveals three peaks with binding energies of 74 eV, 75.1 eV and 75.9 eV, respectively. The peak at 74 eV is attributed to $Al(OH)_3$ [17], the feature of 75.1 eV is assigned to $AlO_x$ and that of 75.9 eV is corresponded to $AlF_3$ [18]. The peaks for Zr 3d at approximately 181.6 eV, 183.4 eV and 184.9 eV were mainly due to the presence of $ZrO_2$ and $ZrF_4$ (Fig. 3(c)) [18]. The detail of F 1s peaks (Fig. 3(d)) reveals two peak structures with binding energies of 685.1 eV and 686.3 eV, respectively. The former is corresponded to $ZrF_4$ and the latter is assigned to $AlF_3$ [18]. The peaks for Ti 2p at approximately 458.7 eV and 464.3 eV are corresponded to $TiO_2$ (Fig. 3(e)) [17,18]. In addition, the C 1s core-level spectrum was curve-fitted into three peak components with binding energies at about 284.07 eV, 284.97 eV and 287.74 eV, which might be attributed to the C-C, C-H and C-N species in the benzimidazole, respectively (Fig. 7(f)) [17,18]. And the O 1s spectrum was curved-fitted into two peaks with binding energies of 530.3 eV and 531.7 eV, which are attributed to $TiO_2$/ $ZrO_2$ and $Al_2O_3$/N-C-O, respectively (Fig. 4(h)) [17,18]. Therefore, the Ti-Zr conversion coating is mainly consist of metallic oxide ($TiO_2$, $ZrO_2$, $Al_2O_3$), metallic fluoride ($ZrF_4$ and $AlF_3$ ) and C-N complex, which is basically consistent with the EDS results.

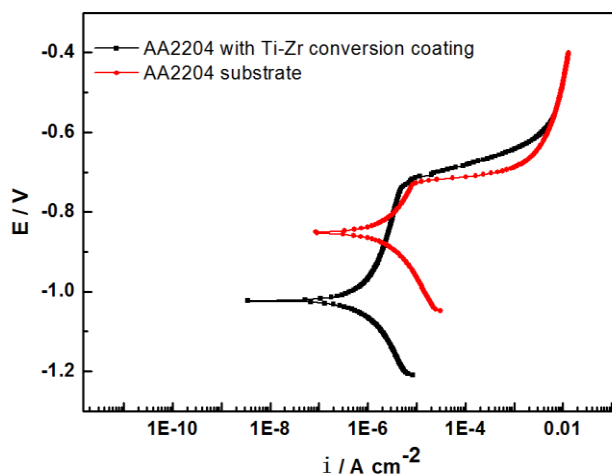*3.2 Electrochemical measurements*



**Figure 4.** Polarization curves for AA2024 with and without Ti-Zr conversion in 5% NaCl solution

**Table 1.** Electrochemical parameters obtained from polarization curves in Figure 4.

|  | Ecorr / V | Icorr / A cm$^{-2}$ | Rp / Ω cm$^2$ | Epit / V | (Epit-Ecorr) / V |
|---|---|---|---|---|---|
| Ti-Zr conversion coating | -1.022 | 5.4484 E-7 | 4.788 E4 | -0.735 | 0.287 |
| AA2024 substrate | -0.852 | 1.9120 E-6 | 1.364 E4 | -0.730 | 0.122 |

Firstly, potentiodynamic polarization measurements were performed to estimate the corrosion resistance of the Ti-Zr conversion coating and Fig. 4 is the Polarization curves of AA2024 without and with Ti-Zr conversion coating in 5% NaCl solution. Specifically, the polarization range is -0.25–0.6 V versus the open circuit potential and the scanning rate was 0.5 mV s$^{-1}$. As shown in Fig. 4, the pitting potential (Epit) of AA2024 without and with Ti-Zr conversion coating is almost the same, however, because of the apparent negative shift the corrosion potential (Ecorr), the passive potential range (Epit-Ecorr) greatly increases for AA2024 with Ti-Zr conversion coating compared with that of AA2024 substrate, indicating a strong passivation and self-healing characteristics for the former [18]. In addition, the cathodic current density of AA2024 with Ti-Zr conversion coating is dropped by two orders of magnitude compared with that of AA2024 substrate under the premise of the similar anodic current density, suggesting the cathodic process is rate controlling step and the corrosion resistance for the former is greatly improved [19].

The fitting results obtained from the polarization curves in Fig. 4 are listed in Table 1. As shown in Table 1, the corrosion potential (Ecorr) is -0.852 V for AA2024 substrate and -1.022 V for AA2024 with Ti-Zr conversion coating. In general, Ecorr of the conversion coating will positively shift compared with that of the Al substrate [9,20], however Ecorr of the Ti-Zr conversion coating negatively shifts about 170 mV compared with that of the AA2024 substrate, which is agree with what Li and her co-workers found in the previous literatures [18,21]. It is surprise to us that there is not any explanation in either of the publications for such the abnormal phenomenon. So several parallel tests were done repeatedly by us and it is confirmed that Ecorr of the AA2024 substrate negatively shifts after the formation of the Ti-Zr conversion coating, which might be attributed to the repressed cathodic reaction resulted from the introduced benzimidazole [14]. The corresponding corrosion current density (Icorr) decreases from 1.9120 to 0.5448μA cm$^{-2}$ after the Ti-Zr conversion treatment, indicating the preferable corrosion resistance. The polarization resistance (Rp) was fitted using CView2 software with the Rp extrapolation in the vicinity of the corrosion potential (±20 mV). Correspondent Rp value increases significantly from 13.64 to 47.88 kΩ cm$^2$, also suggesting a significant improvement in the corrosion resistance for the Ti-Zr conversion coating. In addition, the Epit value of AA2024 with conversion coating or not is almost the same (-0.735 and -0.730 V respectively), indicating the similar pitting-resistance property for both of the two simples before the 168 h NSS test, while the much wider passivation range for the former (almost 2.4 times increased) means a preferable corrosion resistance and self-healing performance at a more negative potential than Epit [9], which is ascribed to the conversion coating containing the cathodic inhibitor of benzimidazole.
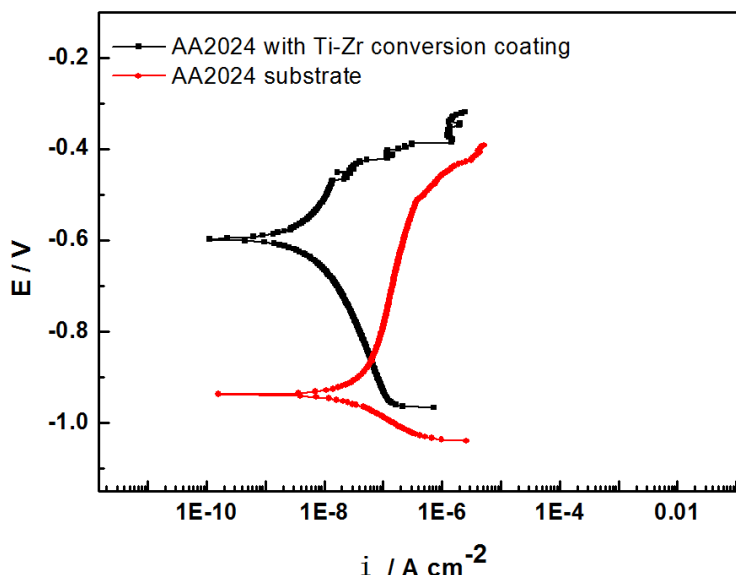
**Figure 5.** Polarization curves for AA2024 with and without the Ti-Zr conversion coating in 5% NaCl solution after the 168 h NSS test

**Table 2.** Electrochemical parameters obtained from polarization curves in Figure 5

|  | Ecorr / V | Icorr / A cm$^{-2}$ | Rp / $\Omega$ cm$^2$ |
|---|---|---|---|
| Ti-Zr conversion coating | -0.597 | 3.342 E-9 | 7.806 E6 |
| AA2024 substrate | -0.937 | 3.436 E-8 | 7.593 E5 |

In spite of the excellent corrosion resistance of AA2024 with Ti-Zr conversion coating compared with that of AA2024 substrate, there is no apparent superiority for the former compared with other chrome-free conversion coating according to the electrochemical parameter in Table 1 [9]. However, the results of the polarization test of AA2024 with Ti-Zr conversion coating after the 168 h NSS test are impressive to us. As shown in Fig. 5, neither polarization curves of AA2024 with and without the Ti-Zr conversion coating especially for the former exhibit an apparent passivation characteristics, instead with the behavior of anodic dissolution of metal. To be specific, the localized corrosion has been occurring under the attack of Cl$^{-1}$ for AA2024 substrate during the NSS test and it is hard to form complete and compact passive film, the generated corrosion products of Al(OH)$_3$ further result in the negative shift of Ecorr for AA2024 (as listed in Table 2). Simultaneously, the newly generated less-complete passive film covered with the corrosion products of Al(OH)$_3$ (see the SEM image Fig. 2) could protect AA2024 substrate from the anodic dissolution to a great extent, so smaller values of Icorr and Rp (34.36 nA cm$^{-2}$ and 0.759 M$\Omega$ cm$^2$) could be obtained for AA2024 substrate after the 168 h NSS test compared with those before the NSS test (1.9120μA cm$^{-2}$ and 13.64 k$\Omega$ cm$^2$). As for AA2024 with Ti-Zr conversion coating, a small amount of corrosion products were generated

after the 168 h NSS test and the original porous structure were well filled with the generated $Al(OH)_3$, which weak the possible sacrifice effect of the Ti-Zr conversion coating and further cause the positive shift of Ecorr. At this time, the Ti-Zr conversion coating with the pore structure filled with $Al(OH)_3$ acts as a high-resistance coating which isolates the substrate and electrolyte to some extent, consequently smaller values of Icorr and Rp (3.342 nA cm$^{-2}$ and 7.806 MΩ cm$^2$) could be obtained for AA2024 with Ti-Zr conversion coating. Such little Icorr and high Rp for AA2024 with chromium-free conversion coating after the 168 h NSS test indicate the Ti-Zr conversion coating prepared in this work is a very promising high-performance chromium-free protective coating for AA2024 [3].
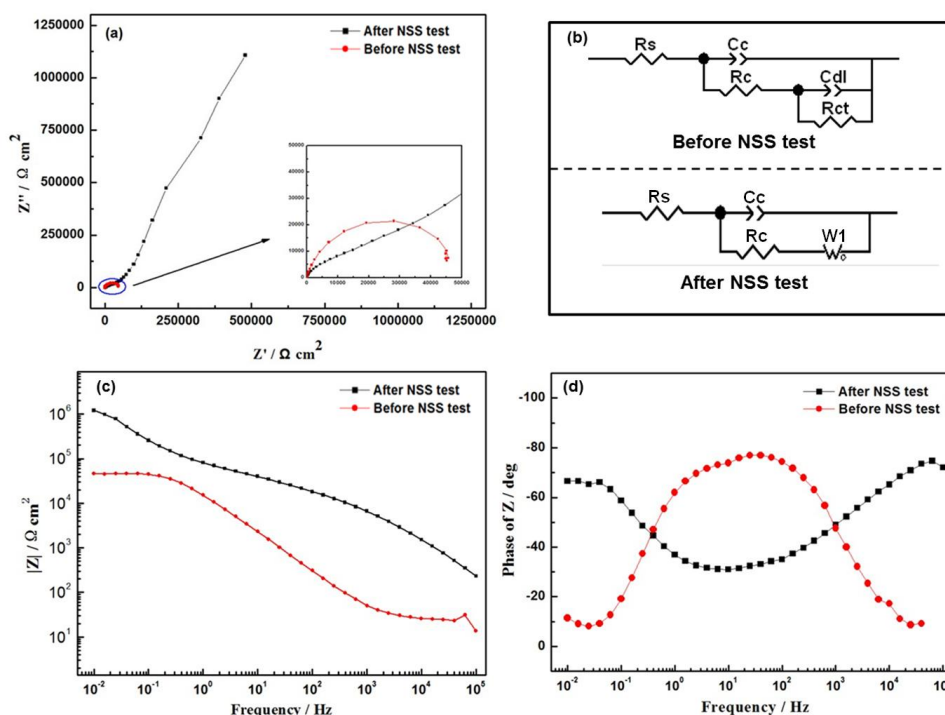


**Figure 6.** Nyquist diagram (a), Bode plots (c-d) of AA2024 Ti-Zr conversion coating in 5% NaCl solution before and after the 168 h NSS test, and the corresponding equivalent circuits (b).

In order to further estimate the electrochemical performance of the Ti-Zr conversion coating, EIS tests of AA2024 with Ti-Zr conversion coating before and after the 168 h NSS test were conducted in 5% NaCl solution. As shown in Fig. 6(a), the nyquist diagram of the Ti-Zr conversion coating before the 168 h NSS test presents a typical semi-cycle during the whole frequency range (Enlarged view in Fig. 6(a)), while the almost overlapped two phase peak at the low-mid frequency in the bode plots (Fig. 6(d)) indicates that there should be two time constants for AA2024 Ti-Zr conversion coating in 5% NaCl solution, which corresponds to two different processes. The first mainly relates with the conversion coating and the second represents electron transfer process, the corresponding equivalent circuit is as shown in Fig. 6(b) [8]. In contrast to that, an arc of a one-fourth circle at high frequency (Enlarged graph in Fig. 6(a)) and a linear part at low frequency could be seen

for AA2024 Ti-Zr conversion coating after the 168 h NSS test (Fig. 6(a)), the former often refers to conversion coating while the latter means a diffusion process, which is consistent with the two peaks in the bode plots (Fig. 6(d)) [3]. In addition, it is worth noting that the magnitude of impedance obtained in the lower frequency region is about 45 k$\Omega$ cm$^2$ for AA2024 before the NSS test (Fig. 6(c)), while that is more than 1 M$\Omega$ cm$^2$ for AA2024 after the NSS test, indicating that the corrosion resistance of the conversion coating improves gradually for a period of time during the NSS test and the improvement might be attributed to the generated passive film (Al$_2$O$_3$) and/or corrosion products (Al(OH)$_3$), which is agree with the SEM and polarization results.

**Table 3.** The fitted EIS parameters obtained from the nyquist plots in Figure 6(a)

|  | Rs / $\Omega$ cm$^2$ | Cc-T / F cm$^{-2}$ | Cc-P / - | Rc / $\Omega$ cm$^2$ | Cdl-T / F cm$^{-2}$ | Cdl-P / - | Rct / $\Omega$ cm$^2$ |
|---|---|---|---|---|---|---|---|
| 0 h | 22.89 | 3.0248E-6 | 0.8994 | 12.13 | 6.5822E-6 | 0.8875 | 41858 |
|  | Rs / $\Omega$ cm$^2$ | Cc-T / F cm$^{-2}$ | Cc-P / - | Rc / $\Omega$ cm$^2$ | W1-R / $\Omega$ cm$^2$ | W1-T | W1-P |
| 168 h | 25.02 | 7.457 E-8 | 0.81806 | 8389 | 157470 | 0.90773 | 0.37969 |

Furthermore, the nyquist plots of AA2024 with Ti-Zr conversion coating before and after the 168 h NSS test can be fitted with the corresponding equivalent circuit in Fig. 6(b). Herein, Rs stands for bulk solution resistance, Cc represents the capacitance of the conversion coating and Rc often relates to its resistance, Cdl is the double layer capacitance of the coating/substrate interface and Rct means the electron transfer resistance for the corrosion reaction, W1 often refers to the Warburg resistance [13]. First of all, the values of Rs for the two samples are almost the same, which is as expected because of the same solution. Secondly, Cc-T for the sample before the NSS test is much larger than that after the NSS test, which is due to the porous structure for the former. It is interesting that the coating resistance is only 12.13 $\Omega$ cm$^2$, indicating the original corrosion resistance of the Ti-Zr conversion coating is not very outstanding and the superiority in the corrosion resistance compared with AA2024 substrate might be mostly attributed to the cathodic inhibitor of benzimidazole. However, the newly generated passive film (Al$_2$O$_3$) and/or corrosion products (Al(OH)$_3$) well filled the porous conversion coating during the NSS test and made the conversion coating a relatively high-resistance protective coating, accordingly Rc of the sample after the NSS test increase to 8389 $\Omega$ cm$^2$. Finally, the porous conversion coating of the sample before the NSS test has little hindering effect on the diffusion process and the electron transfer process is the rate limited step, the corresponding Rct is about 41858 $\Omega$ cm$^2$. But for the sample after the NSS test, the relatively complete and compact conversion coating is formed after the NSS test, which greatly hinders the diffusion process of the corrosion products and makes the diffusion step the rate limited step, and the Warburg resistance is high up to 0.157 M$\Omega$ cm$^2$ at this time. To sum up, all these results are also consistent with the SEM and polarization results.
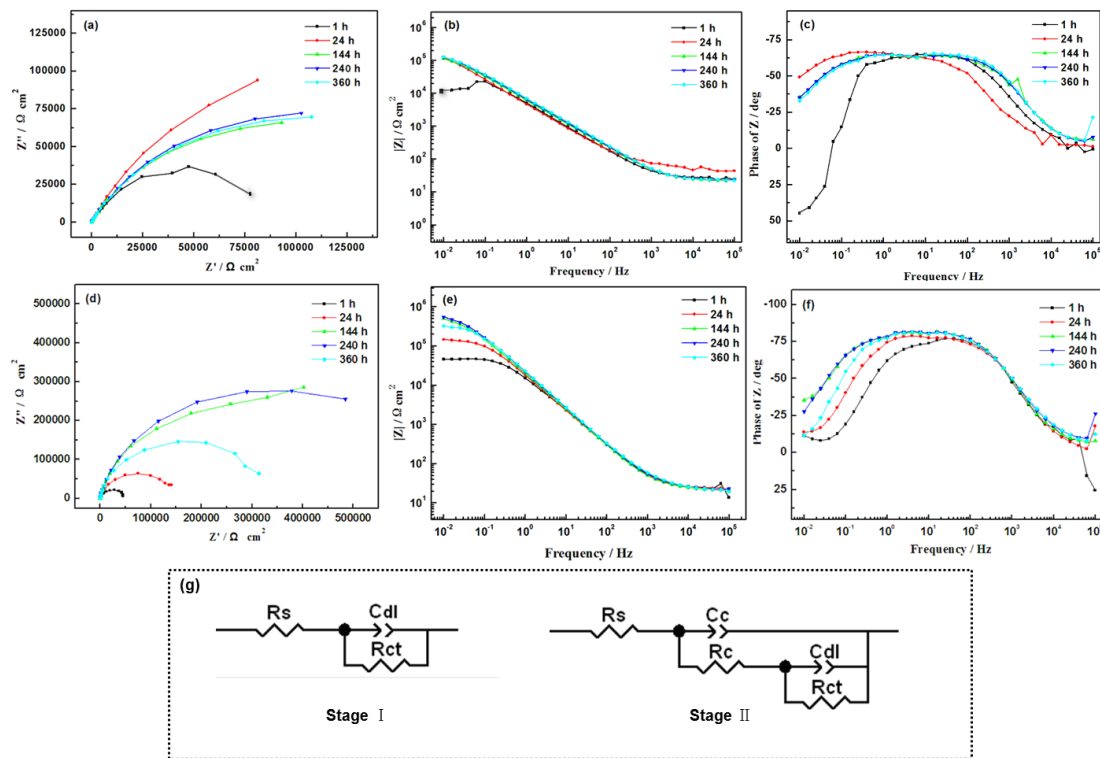
**Figure 7.** Nyquist and bode plots of AA2024 substrate (a-c) and AA2024 with Ti-Zr conversion coating (d-f) in 5% NaCl solution with different immersion time, and the corresponding equivalent circuits for different stages (g)

**Table 4.** The fitted EIS parameters obtained from the nyquist plots in Figure 7(a)

|       | Rs / Ω cm$^2$ | Cc-T / F cm$^{-2}$ | Cc-P / - | Rc / Ω cm$^2$ | Cdl-T / F cm$^{-2}$ | Cdl-P / - | Rct / Ω cm$^2$ |
|-------|------|------|------|------|------|------|------|
| 1 h   | 24.31 | - | - | - | 3.6977E-5 | 0.7949 | 27821 |
| 24 h  | 22.34 | 2.0306E-5 | 0.7584 | 46.73 | 3.2745E-5 | 0.7472 | 383240 |
| 144 h | 21.75 | 3.6172E-5 | 0.7537 | 8225 | 5.4329E-6 | 0.7335 | 183940 |
| 240 h | 22.55 | 2.8560E-5 | 0.7795 | 4051 | 9.6293E-6 | 0.6703 | 210510 |
| 360 h | 22.58 | 2.6511E-5 | 0.7829 | 5740 | 9.8315E-6 | 0.6686 | 198700 |

**Table 5.** The fitted EIS parameters obtained from the nyquist plots in Figure 7(d)

|       | Rs / Ω cm$^2$ | Cc-T / F cm$^{-2}$ | Cc-P / - | Rc / Ω cm$^2$ | Cdl-T / F cm$^{-2}$ | Cdl-P / - | Rct / Ω cm$^2$ |
|-------|------|------|------|------|------|------|------|
| 1 h   | 22.66 | 2.8458E-6 | 0.95083 | 15.52 | 8.9266E-6 | 0.8445 | 50727 |
| 24 h  | 23.27 | 4.9733E-6 | 0.92397 | 43.42 | 5.5677E-6 | 0.86233 | 149910 |
| 144 h | 20.99 | 8.3738E-6 | 0.87323 | 56.98 | 1.5248E-6 | 0.88531 | 609700 |
| 240 h | 21.02 | 6.3164E-6 | 0.87979 | 50.41 | 2.5071E-6 | 0.96132 | 645390 |
| 360 h | 21.66 | 3.9646E-6 | 0.9226 | 53.73 | 4.1745E-6 | 0.9133 | 332020 |

As above-mentioned, the corrosion resistance of the Ti-Zr conversion coating is not so outstanding originally, but improves gradually during the NSS test. Therefore, it is very necessary to clarify the detail change rule of the corrosion resistance. Because the NSS test was conducted for 168 h

according to the ASTM B117, while the immersion test was very convenient to control different immersion times, so the immersion tests of the as-prepared samples with different immersion times were carried out to investigate the changing rule of the corrosion resistance during the long-term immersion process.

As shown in Fig. 7(a), a typical impedance arc in the nyquist plot could be seen for AA2024 substrate immersed in 5% NaCl solution for 1 h, in addition to the only one big and broad phase peak which is observed at the low-mid frequency (Fig. 7(c)), indicating that there is only one time constant for AA2024 substrate immersed in 5% NaCl solution for 1 h, the corresponding equivalent circuit is as shown as the stage. I . in Fig. 7(g). Differently, despite each of the nyquist diagram of AA2024 substrate with different immersion times (24 h, 144 h, 240 h and 360 h) presents a typical impedance arc during the whole frequency range, the almost overlapped two phase peaks at the low-mid frequency in the bode plots (Fig. 7(c)) indicate that there should be two time constants for AA2024 substrate immersed in 5% NaCl solution for no less than 24 h. Similar with the impedance behavior of AA2024 with Ti-Zr conversion coating before the NSS test, the first time constant mainly relates with the conversion coating and the second represents electron transfer process, the corresponding equivalent circuit is as shown as the stage. II .in Fig. 7(g). In addition, the magnitude of the impedance for AA2024 substrate immersed in 5% NaCl solution is almost the same except for that with the immersion time of 1 h, suggesting the newly formed passive film of $Al_2O_3$ and corrosion product of $Al(OH)_3$ could act as the protective coating and they basically keep an equilibrium state when the immersion time is bigger than 20 h.

As for the AA2024 with Ti-Zr conversion coating, despite the second impedance arc is not apparent, there are mainly two impedance arcs could be seen for all the as-prepared samples during the whole frequency range, as shown in Fig. 7(d). Moreover, the almost overlapped two phase peaks at the low-mid frequency in the bode plots (Fig. 7(f)) further demonstrate the two time constants for AA2024 with Ti-Zr conversion coating immersed in 5% NaCl solution, and the equivalent circuit corresponds to that of stage. II .in Fig. 7(g). It is worth noting that the diameter of the corresponding impedance arc firstly increases and then decreases, and the immersion time of 240 h is the turning-point, indicating the corrosion resistance of the conversion coating is improving with the increasing immersion time during the first two-thirds of the immersion period and then keeping a slow reduction. The reason for these might be that under the effect of the cathodic inhibitor benzimidazole, more and more passive films of $Al_2O_3$ were generated with the increasing immersion time during the initial stage (1-144 h), and then the passive film reached a relatively stable state during the middle stage of the immersion period (144-240 h), at last the slightly localized corrosion occurred under the attack of $Cl^{-1}$ and the passive film began to degrade gradually during the later stage (240-360 h). In addition, the magnitude of the impedance for AA2024 with Ti-Zr conversion coating immersed in 5% NaCl solution firstly increases gradually and then begins to decrease, further confirming the proposed viewpoint as above.

Furthermore, the nyquist plots of AA2024 with and without Ti-Zr conversion coating immersed in 5% NaCl solution with different times are also fitted with the corresponding equivalent circuit in Fig. 7(g). The detail meaning of the corresponding parameter is defined as above. As for AA2024 substrate immersed in 5% NaCl solution for 1 h, the equivalent circuit as shown as stage I stands for the direct corrosion process, while the two processes as presented as stage II for AA2024 substrate

immersed in 5% NaCl solution for no less than 24 h represent the protective coating of the newly generated $Al_2O_3$ and $Al(OH)_3$ and corrosion reaction at the interface respectively. As listed in Table 4, the values of Rs for all the samples are almost the same, in accordance with the expectation. Secondly, Cc-T for AA2024 substrate basically changes little (within an order of magnitude) while Rc increases greatly at first and then decreases to some extent with the increasing immersion time, indicating that despite the surface morphology of the protective film keeps unchanged, its main component changes from the initial $Al_2O_3$ to the final $Al(OH)_3$ which make the coating resistance increases firstly and then decreases. Similarly, Cdl-T for AA2024 substrate basically changes little (within an order of magnitude) while Rct increases greatly at first and then decreases to some extent with the increasing immersion time, the reason for those are that Cdl-T and Rct are closely related with the morphology and corrosion resistance of the protective film respectively, as above-mentioned. It is to say, a protective coating composed of the newly generated $Al_2O_3$ and $Al(OH)_3$, which could protect AA2024 substrate from corroding to some extent, will be formed at the surface of AA2024 substrate, while the corresponding corrosion resistance is changing with the transformation of its main compositions.

Regard to AA2024 with Ti-Zr conversion coating, Rs for all the samples is basically equal to those above-mentioned, as listed in Table 5. Secondly, Cc-T for AA2024 with Ti-Zr conversion coating also changes little (within an order of magnitude) with the increasing immersion time, compared with those (almost two orders of magnitude reduced) for AA2024 with Ti-Zr conversion coating before and after the NSS test, indicating the immersion test has less effect on the surface morphology of the conversion coating than the NSS test. The value of Rc only changes within the range of 15.52 to 56.98 $\Omega$ cm$^2$, and little difference in the value of Cdl-T could be observed according to Table 5, both indicate that there is no apparent change in the surface morphology of the conversion coating. Most importantly, the value of Rct is only 50.727 k$\Omega$ cm$^2$ with the immersion time of 1 h, while it increases to 0.6554 M$\Omega$ cm$^2$ with the immersion time increased to 240 h, and then decreases to 0.3320 M$\Omega$ cm$^2$ when the immersion time increases to 360 h. And the increase in Rct with the immersion time less than 240 h mostly ascribes to the newly generated passive film at the surface of AA2024 substrate, which prevents the diffusion of the corrosion products ($Al(OH)_3$), while the reason for the decrease in Rct with the immersion time more than 240 h might be that the cathodic inhibitor of benzimidazole gradually diffuse to the electrolyte and the self-healing ability of the passive film was weakened with the decreasing benzimidazole in the conversion coating.

To sum up, the corrosion resistance of the Ti-Zr conversion coating is not so outstanding at the initial stage, what is worth cherishing is that its anti-corrosion property is gradually improving after it was used for a period of time. Compared with other chrome-free conversion coating, the excellent corrosion resistance of the Ti-Zr conversion coating might be a promising high-performance protective coating for AA2024.

## 4. CONCLUSIONS

A novel non-chromium Ti-Zr based conversion coating on AA2024 was successfully prepared by introducing the cathodic inhibitor of benzimidazole into the Ti-Zr conversion solution. After the

conversion treatment, AA2024 substrate was well covered with the porous Ti-Zr conversion coating which was composed of the micron-sized particles. And the Ti-Zr conversion coating is mainly consist of metallic oxide ($TiO_2$, $ZrO_2$, $Al_2O_3$), metallic fluoride ($ZrF_4$ and $AlF_3$) and C-N complex. There is no apparent corrosion products or detects could be observed during the whole 168 h NSS test, indicating the significantly excellent corrosion resistance for AA2024 with Ti-Zr conversion coating compared with other chrome-free conversion coatings. The electrochemical measurements indicate the corrosion resistance of the Ti-Zr conversion coating is not so outstanding at the initial stage, what is worth cherishing is that its anti-corrosion property is gradually improving. Therefore, the Ti-Zr conversion coating with excellent corrosion resistance might be a promising high-performance protective coating for AA2024 compared with other chrome-free conversion coating.

## References

1. M.A. Baker, J.E. Castle, B. Dunn and J.F. Watts, *Corr. Sci.* 53 (2011) 1214.
2. G. Yoganandan, K.P. Premkumar and J.N. Balaraju, *Surf. Coat. Tech.* 270 (2015) 249.
3. P.S. Coloma, U. Izagirre, Y. Belaustegi, J.B. Jorcin, F.J. Cano and N. Lapen, *Appl. Surf. Sci.* 345 (2015) 24.
4. P. Campestrini, H. Terryn, J. Vereecken and J.D. Wit, *J. Electrochem. Soc.* 151 (2004) B59.
5. S.A. Kulinich, A.S. Akhtar, D. Susac, P.C. Wong, K.C.Wong and K.A.R. Mitchell, *Appl. Surf. Sci.* 253 (2007) 3144.
6. A.S. Hamdy and D.P. Butt, *Surf. Coat. Tech.* 201 (2006) 401.
7. Y.Y. Liu, J.M. Huang and B.J. Claypool, *Appl. Surf. Sci.* 355 (2015) 805.
8. G. Yoganandan, J.N. Balaraju and V.K.W. Grips, *Appl. Surf. Sci.* 258 (2012) 8880.
9. X. Zuo, W.F. Li, S.L. Mu, J. Du, Y.Y. Yang and P. Tang, *Prog. Org. Coat.* 87 (2015) 61.
10. J.H. Nordlien and J.C. Walmsley, *Surf. Coat. Tech.* 153 (2002) 72.
11. M.A. Smit, J.A. Hunter, J.D.B. Sharman, G.M. Scamans and J.M. Sykes, *Corr. Sci.* 46 (2004) 1713.
12. J.J. Zhang, W.F. Li and J. Du, *J. South China Univ. Tech.* 38 (2010) 76.
13. M.A. Smit, J.A. Hunter, J.D.B. Sharman, G.M. Scamans and J.M. Sykes, *Corr. Sci.* 45 (2003) 1903.
14. J.F. Walsh, H.S. Dhariwal, A.G. Sosa, P. Finetti, C.A. Muryn, N.B. Brookes, R.J. Oldman and G. Thornton, *Surf. Sci.* 415 (1998) 423.
15. I. Recloux, M. Mouanga, M.E. Druart and Y. Paint, *Appl. Surf. Sci.* 346 (2015) 124.
16. H.W.Shi, E.H.Han, F.C.Liu and S.Kallip, *Appl. Surf. Sci.* 280 (2013) 325.
17. J.F. Moulder, W.F. Stickle, P.E. Sobol and K.D. Bomben, 2nd ed., Physical Electronics Division, Minnesota, 1992.
18. A.H. Yi, W.F. Li, J. Du and S.L. Mu, *Appl. Surf. Sci.* 258 (2012) 5960.
19. G. Yoganandan, K.P.Premkumar and J.N. Balaraju, *Surf. Coat. Tech.* 270 (2015) 249.
20. N.H. Liu, W.F. Li and J. Du, *Surf. Tech.* 39 (2010) 45.
21. C.X. Wang and X.Y. Yang, *Mater. Prot.* 43 (2010) 36.